Thermoelectric currents in laser induced melts pools

Adrian Lange,[1,a] Andreas Cramer,[2] and Eckhard Beyer[1]

[1]*Institute of Surface and Manufacturing Technology, Technische Universität Dresden, 01069 Dresden, Germany*

[2]*Forschungszentrum Dresden-Rossendorf, P. O. Box 510119, 01314 Dresden, Germany*

Applying an external static magnetic field to laser beam welding may lead to a change in geometry of the weld seam. Since the most common influence of a magnetic field acting on an electrically high conducting fluid is the generation of a Lorentz force, the outcome of such experiments is a strong indication of the presence of electric current in the melt pool. Owing to the static nature of the magnetic field, induction is restricted to the movement of the liquid metal and therefore negligible, leaving thermoelectricity as the sole potential source of current. The present work discloses analytically that the current may indeed originate from a gradient of thermoelectric power. Based on the examples iron and aluminum, key features of the current distribution are determined numerically together with an investigation of the dependence of the distribution on material properties. By carrying out welding experiments in the heat conduction mode, validation is achieved of the thermoelectric source of the current and of basic properties of its contribution. © *2009 Laser Institute of America.*

Key words: thermoelectric current, laser welding, geometry of weld seam

I. INTRODUCTION

Laser beam welding is characterized by high welding speed, low heat input, a high ability to automation, and its ease of combination with other technologies. These features have led to an economical manufacturing technology in many sectors, from automotive, railway, and aircraft constructions to steel and sheet metal constructions. Engineers have been trying to expand the limits of laser beam welding, particularly to achieve higher welding speeds. Besides the desire to improve the economy of the welding process by higher speeds, it is primarily the feasible welding quality which is of greatest significance. That quality is determined by the geometric shape and the strength of the weld seam.

The influence of an external static magnetic field on the quality of the weld seam and therefore on the maintainable welding speed was studied in Refs. 1 and 2. By conducting experiments with fine grained steels and aluminum alloys, a reduction in the so called humping effect, an improvement of the top weld seam quality, and an influence on the cross section of the weld seam were accomplished. From these observed changes in the weld seam the authors of Refs. 1 and 2 concluded that a Lorentz force is acting on the liquid metal in the melt pool and causes these phenomena. Whereas the magnetic field for the Lorentz force stems from the external field, the existence of a internal thermoelectrically induced current was proposed since no other current sources are available.[1,2]

A current on the base of the thermoelectric or Seebeck effect flows if two different metals are in contact with each other, where their contact points have different temperatures.

With respect to the experimental results in Refs. 1 and 2 it is argued that for alloys a thermoelectric voltage exists between the melt and the solidified seam material at one side and between the melt and the base material at the other side. To support that idea of different thermoelectric properties of the base and the solidified seam material, a thermocouple of both materials was built and a voltage with dependence on the temperature difference was measured.[1,2] The measurement of different Seebeck coefficients of steel before and after the heat treatment generating martensitic transformations[3,4] adds further arguments to support the explanation in Refs. 1 and 2.

Based on these experimental facts, it is plausible that in the melt pool a thermoelectrically induced current density exists. The aim of this work is to calculate and to analyze this current density, its dependence on material properties, and relate the results to the assumptions in Refs. 1 and 2 as well as to welding experiments.

II. SYSTEM EQUATIONS AND SOLUTION IN TWO DIMENSIONS

A system is considered, where a laser beam with radius R and a velocity v in x direction welds a thin metal sheet, i.e., its planar dimensions are much larger than its thickness. It is assumed that the stationary regime of welding is reached. Following Refs. 5 and 6, the thermoelectric current density $\mathbf{j}$ is caused by gradients in the chemical potential μ and the temperature T,

$$\mathbf{j} = \frac{\sigma}{e} \operatorname{grad} \mu - \alpha\sigma \operatorname{grad} T. \tag{1}$$

The electrical conductivity is denoted by σ, the elementary charge is denoted by e, and α is either called thermoelectric power or Seebeck coefficient. Since the stationary case is

―――――――――――――――
[a]Electronic mail: adrian.lange@tu-dresden.de

considered and the magnetization due to the magnetic field **H**, induced by **j**, is negligible in liquid metals, the two relevant Maxwell's equations, rot **H** = **j** and div **H** = 0, reduce to a Poisson equation for the z component of **H**,

$$\Delta H_z = \sigma \left(\frac{\partial \alpha}{\partial x} \frac{\partial T}{\partial y} - \frac{\partial \alpha}{\partial y} \frac{\partial T}{\partial x} \right). \tag{2}$$

The spatial dependence of α and T is restricted to two dimensions which corresponds to the welding of thin metal sheets. Equation (2) has to be supplemented with the appropriate boundary condition,

$$j_r|_{r=R} = \left. \frac{1}{R} \frac{\partial H_z}{\partial \phi} \right|_{r=R} = 0, \tag{3}$$

i.e., there is no current flow across the area, where the material is vaporized. With the solution for $\bar{H}_z$ one can calculate the components of the current density,

$$\bar{j}_x(\bar{x}, \bar{z}) = \frac{\partial \bar{H}_z}{\partial \bar{y}} = \bar{\sigma} \int_{r=1}^{\infty} \int_{\phi=0}^{2\pi} \frac{\partial G}{\partial \bar{y}} (\bar{x}, \bar{y}; r \cos \phi, r \sin \phi) F$$

$$(r \cos \phi, r \sin \phi) r dr d\phi, \tag{4}$$

$$\bar{j}_y(\bar{x}, \bar{y}) = -\frac{\partial \bar{H}_z}{\partial \bar{x}} = -\bar{\sigma} \int_{r=1}^{\infty} \int_{\phi=0}^{2\pi} \frac{\partial G}{\partial \bar{x}} (\bar{x}, \bar{y}; r \cos \phi, r \sin \phi)$$

$$F(r \cos \phi, r \sin \phi) r dr d\phi. \tag{5}$$

G is the corresponding Green's function (see Ref. 7) and the function F is the right hand side of Eq. (2). Dimensionless quantities are denoted by a bar, where all lengths are scaled with the laser beam radius R, the temperature with $(T_v - T_a)$, the conductivity with σ_{ref}, the Seebeck coefficients with α_{ref}, and the magnetic field with $\alpha_{ref} \sigma_{ref}(T_v - T_a)$. T_v is the vapor temperature of the material, T_a the ambient temperature, and σ_{ref} as well as α_{ref} are pragmatically chosen reference values for the conductivity and the Seebeck coefficients. The solution for the temperature field of the problem at hand is given in Ref. 8 and contains the dimensionless Péclet number, Pe $= (Rv)/\kappa$, which relates the convective heat transport to the conductive one. κ is the thermal conductivity of the material. In the course of this work the temperature field will be cal-
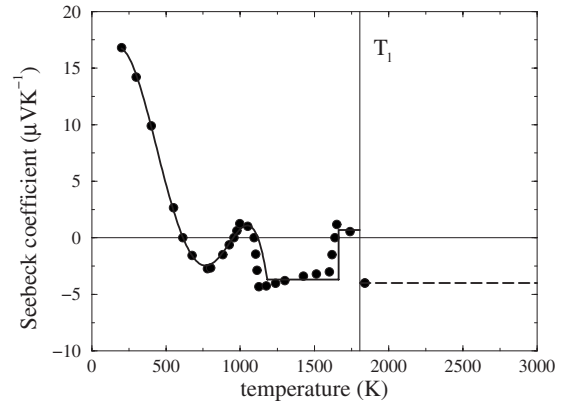

FIG. 1. Seebeck coefficient of iron α^{Fe} versus the temperature T. The measured data of Refs. 9–11 are denoted by filled circles. A fit up to the melting temperature T_l is given by the solid line. $\alpha^{Fe}(T)$ in the liquid phase is modeled by a constant value (long-dashed line).

culated for different Péclet numbers, which reflect different materials as well as different welding conditions.

As the last necessary quantity for the determination of **j**, the Seebeck coefficient with its dependence on temperature and space has to be known. Since the experiments in Ref. 1 were conducted for steel and aluminum alloys, the pure metals iron and aluminum are selected for an analysis which will be presented in the next two consecutive sections.

III. ANALYSIS FOR IRON

Measurements for the Seebeck coefficient of iron are only few, not very recent, and limited to the solid phase with the exception of one data point. Blatt et al.[9] measured α^{Fe} from nearly zero Kelvin up to $T_{\alpha\gamma} = 1183$ K, the temperature for the transition from α-iron to γ-iron. More than two decades later, Vedernikow and Burkov[10] presented data for α^{Fe} from 550 K until close to the melting temperature T_l = 1807 K. To the best of our knowledge, Enderby and Dupree[11] measured the only value of α^{Fe} in the liquid phase at $T = 1840$ K. All these data are summarized in Fig. 1 (filled circles) and show that the temperature dependence is nonmonotonic with discontinuities at the phase transition temperatures $T_{\alpha\gamma}$ and $T_{\gamma\delta} = 1663$ K.[12] This nonmonotonic behavior is described by a fit function (thick solid line),

$$\alpha^{Fe}(T) = \begin{cases} \alpha_4 = a_0 + a_1 T + a_2 T^2 + a_3 T^3 + a_4 T^4 + a_5 T^5, & 200 \text{ K} \leq T < T_{\alpha\gamma} \\ \alpha_3 = -\frac{3691}{1000} \frac{\mu V}{K}, & T_{\alpha\gamma} \leq T \leq T_{\gamma\delta} \\ \alpha_2 = \frac{7}{10} \frac{\mu V}{K} - \alpha_3, & T_{\gamma\delta} < T < T_l \\ \alpha_1 = -\frac{4}{10} \frac{\mu V}{K} - \alpha_2, & T_l \leq T < T_v, \end{cases} \tag{6}$$

where a third discontinuity appears at T_l, the transition tem- perature from the solid to the liquid phase, which is also
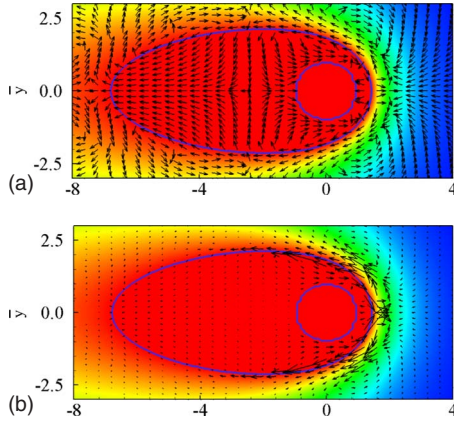
FIG. 2. Current density distribution $\overline{\mathbf{j}}/\overline{\sigma}$ (black arrows) and temperature $\overline{T}$ (color online) for iron with Pe=1. Chart (a) points out the structure of the $\overline{\mathbf{j}}$-field by arrows of uniform length. In chart (b) the length of the arrows is given by the strength of $\overline{\mathbf{j}}$. Areas of high temperature are indicated by the central dark region (red online), areas of lower temperature by the right dark region (blue online). The inner (outer) solid line indicates the isotherm of T_l (T_v).

FIG. 3. Current density distribution $\overline{\mathbf{j}}/\overline{\sigma}$ (black arrows) and temperature $\overline{T}$ (color online) for iron with Pe=4 and α_1=const. The distribution consists of two distinctive parts each with a different major direction of the current density as in the case of Pe=1.

observable for other pure metals.[13] For $T > T_l$, $\alpha^{Fe}(T) = \alpha_1$ is modeled by a constant value equal to the one measured in Ref. 11 (see long-dashed line in Fig. 1). A linear decreasing behavior of α_1 was also tested. Since those results differ only very weak from the case of a constant value, all calculations for iron are restricted to the case α_1=const. The value of $a_0, \ldots, a_5$ used in the temperature dependence of α_4 is given in the Appendix.

For the spatial distribution of the Seebeck coefficient it is exploited that the isotherms of the temperature field can be well approximated by ellipses. Therefore the ansatz

$$\alpha^{Fe}(x,y) = \alpha_1 \exp\left\{-2\left[\frac{(\overline{x}-\overline{x}_{ins})^2}{a^2} + \frac{\overline{y}^2}{b^2}\right]^n\right\} + \alpha_2$$
$$\times \exp\left\{-2\left[\frac{(\overline{x}-\overline{x}_{in})^2}{c^2} + \frac{\overline{y}^2}{d^2}\right]^n\right\} + \alpha_3$$
$$\times \exp\left\{-2\left[\frac{(\overline{x}-\overline{x}_{out})^2}{e^2} + \frac{\overline{y}^2}{f^2}\right]^n\right\} + \alpha_4\left(1-\right.$$
$$\left.\exp\left\{-2\left[\frac{(\overline{x}-\overline{x}_{out})^2}{e^2} + \frac{\overline{y}^2}{f^2}\right]^n\right\}\right) \quad (7)$$

is made. Besides the temperature dependence via the coefficients α_i the chosen ansatz contains an explicit spatial dependence of α^{Fe}. Such an ansatz is a direct consequence of the use of pure metals instead of alloys and leads to a nonzero thermoelectric current. With the knowledge of the Seebeck distribution (7) and the temperature distribution one can calculate the two components of the thermoelectrically induced current density [Eqs. (4) and (5)]. Figure 2 presents the distribution of the scaled current density $\overline{\mathbf{j}}/\overline{\sigma}$ (black arrows) and of the temperature $\overline{T}$ (color online) for Pe=1. This Péclet number corresponds to a rather slow welding velocity of about $v \sim 0.5$ m/min at a laser radius of $R=600$ μm using the typical thermophysical properties of iron.[14] In chart (a) the arrows have a uniform length to point out the structure of
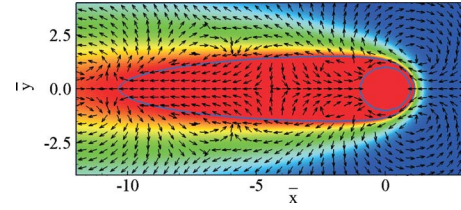
the $\mathbf{j}$-field, whereas in chart (b) the length of the arrows corresponds to the strength of the current density. Areas of high temperature are indicated by the central dark region (red online), areas of lower temperature by the right dark region (blue online) and two thick lines indicate the isotherm of T_v (inner one) and of T_l (outer one). The melt pool is divided into two parts, where in the rear part ($-6.8 \lesssim \overline{x} \lesssim -2.5$) $\mathbf{j}$ is directed predominantly to the rear of the pelt pool. In contrast, in the front part ($-2.5 \lesssim \overline{x} \lesssim 1.4$) $\mathbf{j}$ is directed predominantly to the front, i.e. in the direction of welding. Vortices of $\mathbf{j}$ can been detected at the isotherm of melting and in the front part of the keyhole, where T_v and T_l are rather close to each other. The appearance of a vortex at the latter place is confirmed by the earlier results of Paulini et al.,[6] who found the same phenomenon in the case of two different materials. The region in front of the keyhole experiences the steepest temperature gradient and is therefore also the region of the strongest current density as the longer arrows in the right column show. The correlation between steep temperature gradients and strong current densities is evident since $\mathbf{j}$ is a linear function of grad T [see Eq. (1)].

If one increases the welding velocity to a value of $v =2$ m/min, a Péclet number of $\simeq 4$ results with the corresponding current distribution presented in Fig. 3. It consists again of two distinctive parts each with a different major direction of the current density, whereas the temperature field is elongated (compare Fig. 3 with Fig. 2 and note the different scale at the $\overline{x}$ axis). Thus a change in Pe influences only the temperature field, but not the features of the current density distribution.

IV. ANALYSIS FOR ALUMINUM

Beside a steel alloy, described by pure iron, an aluminum alloy was welded in Ref. 1. Therefore aluminum as second pure metal is chosen to model thermoelectrically induced currents in this type of alloys. Rosenfeld and Timsit[15] measured the Seebeck coefficient α^{Al} in the temperature range between 320 and 780 K, where the authors allow the extrapolation of the fitting equation,

$$\alpha_s^{Al} = -0.8 \; \mu V/K - (1.9 \times 10^{-3} \; \mu V/K^2)T \quad 320 \; K < T$$
$$\leq T_l, \quad (8)$$

up to the melting temperature of T_l=933 K. In the liquid phase of aluminum Auchet and Terzieff[16] determined the temperature coefficient of α_l^{Al} which is assumed to be con-

(a)

(b)
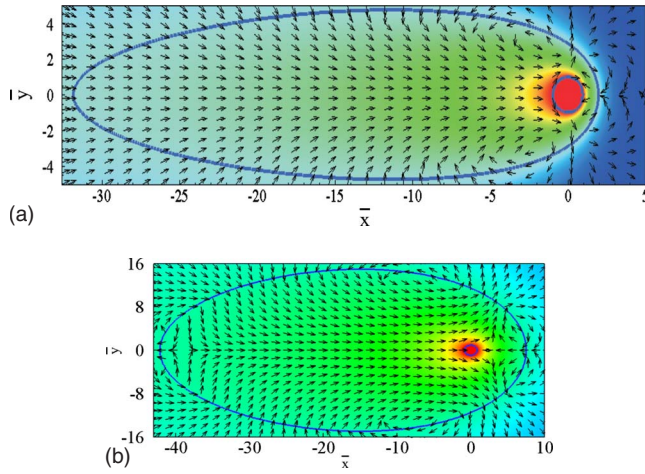
FIG. 4. Current density distribution $\bar{\mathbf{j}}/\bar{\sigma}$ (black arrows) and temperature $\bar{T}$ (color online) for Pe=1 (a) and Pe=0.1 (b) for aluminum. To point out the homogeneous flow of the distribution all arrows have a uniform length. More details are described in the text. The use of the colors is as in Fig. 2 and note the different scales at the $\bar{x}$ and $\bar{y}$ axes.

stant in the entire liquid phase. Therefore the Seebeck coefficient is modeled in this phase as

$$\alpha_l^{Al} = 0.454 \ \mu V/K - (3.4 \times 10^{-3} \ \mu V/K^2)T, \quad T_l \leqslant T$$
$$< T_v = 2740 \ K. \tag{9}$$

Following the method introduced for iron, the spatial distribution of the Seebeck coefficient is given by

$$\alpha^{Al}(x,y) = \alpha_l^{Al} \exp\left\{ -2\left[\frac{(\bar{x}-\bar{x}_{ins})^2}{a^2} + \frac{\bar{y}^2}{b^2} \right]^n \right\} + \alpha_s^{Al}\left(1 \right.$$
$$\left. - \exp\left\{ -2\left[\frac{(\bar{x}-\bar{x}_{ins})^2}{a^2} + \frac{\bar{y}^2}{b^2} \right]^n \right\} \right). \tag{10}$$

Figure 4 shows the distribution of the current density $\bar{\mathbf{j}}/\bar{\sigma}$ (black arrows) and of the temperature $\bar{T}$ (color online) for Péclet numbers of 1 (a) and of 0.1 (b). Besides the case Pe =1 a lower Péclet number of 0.1 is chosen because aluminum is welded often at a lower velocity due its high thermal conductivity. Both distributions show a more homogeneous flow pattern of the current density than in melted iron. For both Péclet numbers the direction of $\mathbf{j}$ is uniform over nearly the entire melt pool and directed towards the front of the melt pool, i.e. in the direction of welding. A uniform orientation confirms the assumption of Kern et al.[1] but the calculated direction towards the front of the melt pool is opposite to the orientation assumed in Ref. 1.

So far in all calculation the properties of the solidified weld seam material have been excluded. In Refs. 1 and 2 a thermocouple was build from that material and from the base material. The measured voltage at applied temperature differences indicates that the Seebeck coefficient of the solidified weld seam material is different from that of the base material. This observation is supported by studies of Yoshida and co-workers,[3,4] who found that the value of the Seebeck coefficient depends on the amount of martensite, which forms during the cooling of steel after welding. Thus a Seebeck coefficient of the weld seam α_{seam}^{Al} is now included, where
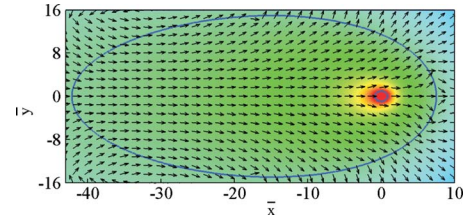

FIG. 5. Current density distribution $\bar{j}/\bar{\sigma}$ (black arrows) and temperature $\bar{T}$ (color online) for aluminum with weld seam at Pe=0.1. Compared to aluminum without a weld seam [Fig. 4(b)] the flow pattern is more homogeneous, i.e., the two vortices at the front and at the rear of the pool disappeared. The use of the colors is as in Fig. 2.

three principal relations are possible: (i) $\alpha_{seam}^{Al} > \alpha_s^{Al} > \alpha_l^{Al}$, (ii) $\alpha_s^{Al} > \alpha_{seam}^{Al} > \alpha_l^{Al}$, and (iii) $\alpha_s^{Al} > \alpha_l^{Al} \approx \alpha_{seam}^{Al}$. Since no qualitative differences in the current distribution between the three cases appeared, only the results for the first one are shown here.

Remarkable in the current distribution including the Seebeck coefficient of the weld seam, see Fig. 5, is that the two vortices at the front and at the rear of the weld pool disappear. That means that the weld seam homogenizes the flow pattern of the current distribution in the melt pool. Therefore this current distribution is even closer to the assumption in Ref. 1 if one ignores the opposite sign of the major direction of $\mathbf{j}$.

V. DISCUSSION AND CONCLUSION

Motivated by welding experiments with alloys, the distribution of thermoelectrically induced current densities is calculated in melt pools of iron and aluminum which are model fluids to approximate the features of the alloys used in the experiments. For iron, the melt pool divides into two parts each with a different major direction of the current density: in the front part it points in the direction of welding, in the rear part opposite to it. In aluminum the flow pattern is more homogeneous than in iron, i.e., there is only one major direction over the entire melt pool which points in the direction of welding.

To confirm the general results of the numerical calculation, a validation by real welding experiments with external magnetic fields is desirable. Such a desire has to cope with the fact that the only real measurable quantity, the geometry of the cross section of the weld seam, bears no direct traces of the current density distribution. It is rather so that the cross section results from a flow field in the melt pool during solidification, whereas the flow field is affected by the Lorentz force density distribution which on its part is governed by the current density distribution. That multiple inverse problem emphasizes the need for numerical analyses as presented in this work. Also, it indicates that experiments show indirectly the generic features of the current density distribution.

To ensure the thermoelectric origin of the latter as the sole cause, the tested alloy inconel is welded by a Nd:YAG laser (Rofin-Sinar DY044) in the heat conduction mode. During that mode of welding the absence of metal plasma excludes it as a current source. The heat conduction mode is
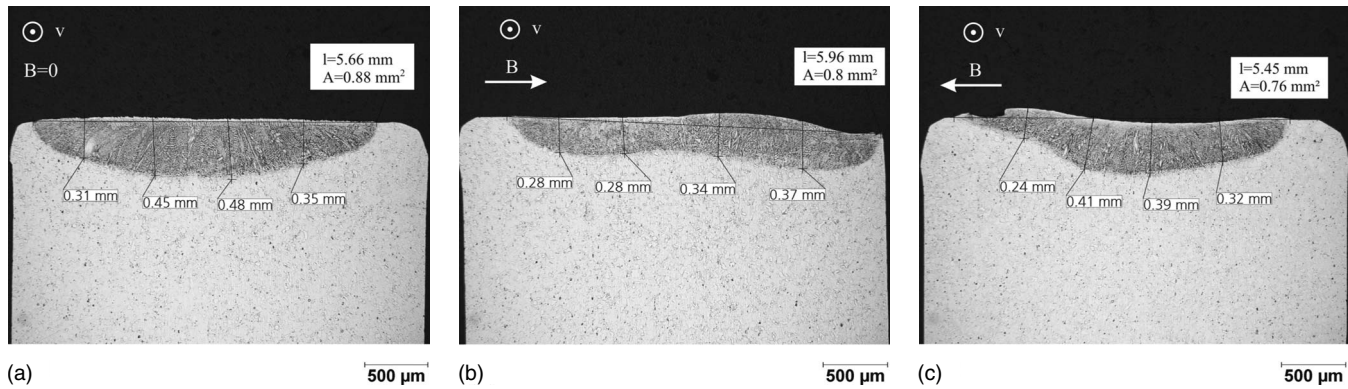
FIG. 6. Weld seam cross section of an inconel sheet (4 mm thick) if welded without (a) and with a magnetic induction B of two different orientations [(b) and (c)]. The radius of the laser bean at the surface of the sheet is 550 μm. The direction of the welding velocity v is indicated by ⊡. The circumference l and the area A of the cross section are given as well as the depth at different positions. The cause of the changes in the cross section is explained in the narrative.

accomplished by operating the laser at a power of 1500 W, by a focal length of the optical system in the welding head of 200 mm, and by a collimation of the same size. The radius of the optical fibre is 300 μm. In order to have clear observable changes in the geometry of the weld seam, the inconel sheet of a thickness of 4 mm is sandwiched between cobalt plates which increase the gradient in the Seebeck coefficient. That causes an amplification of the current and the Lorentz force density, respectively. Importantly, the chosen welding parameters are such that the laser induced melt pool is restricted entirely to the inconel sheet. By varying the vertical distance between the surface of the work piece and the welding head, the influence of the spot size of the laser beam on the work piece is studied. Figures 6 and 7 show the weld seam of the inconel sheet if welded with a radius of the laser beam of 550 μm and 510 μm, respectively.

Figure 6 displays the weld seam of the inconel sheet at welding without (a) and with [(b) and (c)] a magnetic induction B. Chart (a) displays a wide and flat weld seam, the typical geometric feature at welding in the heat conduction mode. For the direction of B in chart (b), the convex shape of the surface of the weld seam is noticeable in contrast to the flat shape for B=0. By reversing the direction of B, consequently a concave shape is formed [see Fig. 6(c)]. These changes of the shape are also observable when welding with a smaller radius (see Fig. 7). For an induction pointing to the

right (left), the former flat surface becomes convex (concave). The smaller radius, i.e., the higher power density causes a clear distinguishable seam root. That feature of welding without a magnetic induction [Fig. 7(a)] disappears completely for the direction of B in Fig. 7(b) and is reduced by 20% for the reversed direction. Drastic changes of this kind reflect the massive changes in the flow field of the melt pool.

A further sign of the changed flow field are the reductions in the depth in the central part of the weld seam. Whereas for $R=550$ μm the depth shrinks by 30% and 10%, respectively [Figs. 6(b) and 6(c)], the welding with $R=510$ μm is accompanied by reductions of 60% and 20%, respectively [Figs. 7(b) and 7(c)]. The experiments show that a reduction in the radius of the laser beam by nearly 10% doubles the reduction in the central part of the weld seam.

The changes in the shape as well as the reduction in the depth are explainable by a spatially varying Lorentz force distribution, the governing current distribution of which is directed out of the plane in the central part, i.e. in the direction of welding. Since the magnetic induction is homogeneous, it does not contribute to the spatial variation of the Lorentz force. Thus the observed changes in the weld seam confirm a major result in the presented numerical calculations. They also indicate that more and precise measurements of the Seebeck coefficients are needed, particularly over a
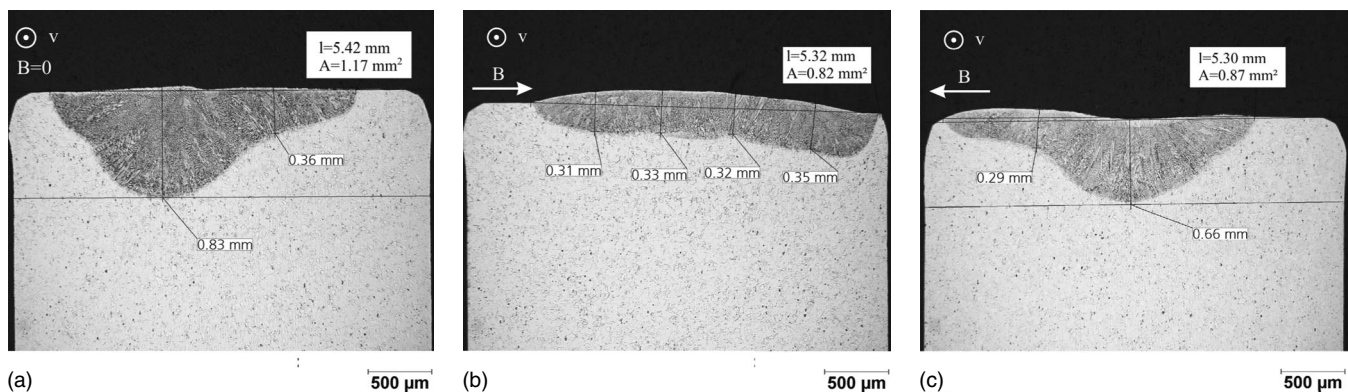

FIG. 7. Weld seam cross section of an inconel sheet under welding conditions as in Fig. 6 with the exception of a smaller radius of the laser beam of 510 μm. The circumference l and the area A of the cross section are given as well as the depth at different positions.

wide temperature range in the liquid phase of metals and alloys. Other perspectives are the extension of the numerics to three dimensions and forthcoming welding experiments with different material combinations in order to improve the weld seam.

ACKNOWLEDGMENTS

APPENDIX

The values of the coefficients $a_0, \dots, a_5$ for α_4 in Eq. (6) are

$$a_0 = \frac{766}{100}\frac{\mu V}{K}, \tag{11}$$

$$a_1 = \frac{1083}{10\,000}\frac{\mu V}{K^2}, \tag{12}$$

$$a_2 = -\frac{367}{1\,000\,000}\frac{\mu V}{K^3}, \tag{13}$$

$$a_3 = \frac{2379}{10\,000\,000\,000}\frac{\mu V}{K^4}, \tag{14}$$

$$a_4 = \frac{1449}{10\,000\,000\,000\,000}\frac{\mu V}{K^5}, \tag{15}$$

$$a_5 = -\frac{13}{1\,000\,000\,000\,000\,000}\frac{\mu V}{K^6}. \tag{16}$$

[1] M. Kern, P. Berger, and H. Hügel, "Magneto-fluid dynamic control of seam quality in CO_2 laser beam welding," Weld. J. (Miami, FL, U.S.) **79**, 72s (2000).

[2] M. Kern, "Gas- und magnetofluiddynamische Maßnahmen zur Beeinflussung der Nahtqualität beim Laserstrahlschweißen," *Laser in der Materialbearbeitung-Forschungsberichte des IFSW* (B. G. Teubner, Stuttgart, 1999).

[3] I. Yoshida, T. Ona, K. Iino, and D. Monma, "Martensitic transformations studied by the measurement of thermoelectric properties," In *Proceedings 20th International Conference on Thermoelectrics* (Piscataway, New York, 2001), pp. 495–498.

[4] I. Yoshida, "Internal friction of metastable austenitic stainless steel SUS 303," J. Phys. (Paris), Colloq. **6**, 385 (1996).

[5] R. D. Barnard, *Thermoelectricity in Metals and Alloys* (Taylor & Francis, London, 1972).

[6] J. Paulini, G. Simon, and I. Decker, "Beam deflection in electron beam welding by thermoelectric eddy currents," J. Phys. D: Appl. Phys. **23**, 486 (1990).

[7] A. G. Butkovskiy and L. W. Longdon, *Green's Functions and Transfer Functions Handbook* (Ellis Horwood, Chichester, 1982).

[8] W. Schulz, "Die Dynamik des thermischen Abtrags mit Grenzschichtcharakter," Habilitation thesis, RWTH Aachen, 1999.

[9] F. J. Blatt, D. J. Flood, V. Rowe, and P. A. Schroeder, "Magnon-drag thermopower in iron," Phys. Rev. Lett. **18**, 395 (1967).

[10] M. V. Vedernikov and A. T. Burkov, "High-temperature thermopower of iron and dilute iron-vanadium alloys," J. Phys. F: Met. Phys. **18**, 465 (1988).

[11] J. E. Enderby and B. C. Dupree, "The thermoelectic power of liquid Fe, Co and Ni," Philos. Mag. **35**, 791 (1977).

[12] M. V. Vedernikov, "The thermoelectric powers of transition metals at high temperature," Adv. Phys. **18**, 337 (1969).

[13] J. A. Shercliff, "Thermoelectric magnetohydrodynamics," J. Fluid Mech. **91**, 231 (1979).

[14] A. Robert and T. Debroy, "Geometry of laser spot welds from dimensionless numbers," Metall. Mater. Trans. B **32**, 941 (2001).

[15] A. M. Rosenfeld and R. S. Timsit, "Thermopower of dilute aluminium alloys and α-brass at elevated temperatures," Philos. Mag. B **49**, 111 (1984).

[16] J. Auchet and P. Terzieff, "The effect of Ti, V and Cr impurities on the transport properties of liquid aluminium," J. Alloys Compd. **261**, 295 (1997).